B.G. Thomas and S.P. Vanka, 2002 NSF Design, Service, Manufacturing and Industrial Innovation Research Conf., San Juan, Puerto Rico, January 7-10, 2002.

Flow Dynamics and Inclusion Transport in Continuous Casting of Steel

Thomas, Brian G., and Vanka, S.P.

University of Illinois at Urbana-Champaign
Mechanical and Industrial Engineering.
1206 West Green Street, Urbana, IL 61801
Ph: 217-333-6919, 217-244-8388; Fax: 217-244-6534;
Email: bgthomas@uiuc.edu, s-vanka@uiuc.edu

Abstract

The quality of continuous cast steel is greatly affected by fluid flow in the mold region, especially involving transient phenomena and the transport of inclusion particles. As part of a long-term effort to develop and apply comprehensive models of these and other phenomena, this paper reports on studies to evaluate the relative accuracy of models of three different fluid flow phenomena in continuous casting through comparison with measurements.

Firstly, transient flow simulations of velocities in the mold region previously validated with digital particle image velocimetry (PIV) measurements in a single phase water model are applied to inclusion transport. Specifically, particle trajectories are calculated in transient flow fields resulting from Large Eddy Simulations (LES). The results are compared with water model measurements to study the distribution and flotation removal of inclusion particles. The LES model was able to match the measurements both qualitatively and quantitatively. Secondly, steady, multiphase flow computations are compared with flow patterns observed in both a water model and an operating steel caster with argon gas injection. For the same conditions, the water model and steel caster produced very different flow behavior. The computational model was able to match the measured flow patterns in both cases. Thirdly, transient LES simulations of impinging jets are performed and applied to predict heat transfer to surface. This is important for the prediction of shell thinning and breakouts. The angle of jet impingement against the narrow face also appears to have an important influence on the fraction of inclusion particles transported down deep into the caster, where they may become entrapped to form defects.

This work suggests that computational flow modeling has the potential to match real processes as well or better than water models, especially when complex related phenomena such as particle motion and multiphase flow are involved. The models will be further improved and applied in future parametric studies.

1. INTRODUCTION

Continued viability of the high-volume low-profit-margin steel industry depends upon improved efficiency and consistent steel quality, relative to low cost imports. Lowering defects from internal inclusions is one way to achieve this, while simultaneously improving steel minimum strength, fatigue life, surface appearance, yield and energy efficiency (from reduced rejects). Even a one percent reduction in yield loss would save about $100 million per year, (based on the roughly 100 million tons of steel produced each year the U.S. [1] and $100 per ton net cost of scrapping). Moreover, reliable lowering of inclusion entrapment could allow thinner gage products (with associated weight and energy savings) and could reduce the need for costly secondary refining steps, such as vacuum arc refining and electroslag remelting. Thus, there are tremendous economic, environmental and safety incentives for understanding how to lower the inclusion content of the steel.

Continuous casting produces 96% of the steel manufactured in the U.S. [1] and is the last, and most important, processing step where inclusions can either be generated or removed. Plant observations have found that many serious quality problems, including inclusion entrapment, are directly associated with the flow pattern in the mold.[2] Defects caused by nonoptimal fluid flow are even more important to the nearer-net-shape thin-slab casting processes, which are starting to transform the industry.[3] This is because higher velocities are required through a smaller inlet nozzle to cast a thin section slab with the same throughput. Thus, design and control of the fluid flow pattern in the continuous casting mold to minimize inclusions is of crucial importance to the steel industry.

The flow pattern in the mold can be controlled by many variables, including the nozzle and mold geometry, submergence depth, steel flow rate, argon injection rate, electromagnetic stirring, and flux layer properties. Many of these parameters are easy and inexpensive to change and yet have a profound influence on flow and corresponding quality. Currently, flow pattern design is done through trial and error, based on qualitative experiments with water models, plant trials, and the plant operator's experience with defects. Identifying an optimal flow pattern is very difficult, because the fundamental relationship between flow pattern and inclusion entrapment has not been quantified. Thus, each casting operation requires its own expensive experiments, and old defects often reappear when changes in the process occur. With so many different operations and new processes to optimize, the industry can no longer afford this approach.

In previous studies, the principal investigators have applied computational models to increase understanding of flow in the continuous casting mold, using both steady-state[4-21] and transient simulations.[22-29] The reliability of these models to predict flow has been demonstrated through comparison with both water models[9-11, 16, 19, 20, 24, 27, 28] and flow measurements in an operating steel caster.[26, 28] The next step is to apply these models to investigate fundamentally, the associated transport and entrapment of inclusion particles and to determine quantitative relationships between flow pattern control parameters (eg. nozzle geometry) and particle entrapment. The current research is concerned with developing and applying such computations, combined with physical water modeling studies to validate the models and to provide

further insight. Finally, plant trials are conducted to further validate the models, and to test proposed improvements. The results of this study should benefit to the steel industry by leading to increased fundamental understanding of inclusion entrapment, and to improvements in design and operating conditions that improve flow pattern in the continuous casting strand and lower costly defects.

2. THE PROCESS

A schematic of part of the continuous casting process is depicted in Figure 1.[30] Steel from the ladle flows through the "tundish," and then it exits down through a ceramic Submerged Entry Nozzle (SEN) and into the mold. Here, the steel freezes against the water-cooled copper walls to form a thin solid shell, which is continuously withdrawn from the bottom of the mold at a "casting speed" that matches the flow of the incoming metal. Flow through the SEN is gravity driven by the pressure difference between the liquid levels of the tundish and the mold top free surfaces. The flow rate is controlled (using feedback from a level sensor) to maintain the liquid level in the mold as constant as possible. In one method, a "stopper rod" extends down through the tundish to partially plug the exit. In another method, a "slide gate" blocks off a portion of the SEN pipe section by moving a disk-shaped plate through a horizontal slit across the entire SEN. Such flow adjustment methods allow for independent control of casting speed and metal level, and are essential for stopping the flow of molten steel if the operation must be abruptly terminated. The submerged nozzle protects the molten steel from exposure to air, which helps to avoid reoxidation and inclusion formation. Together with the casting speed, mold geometry, argon gas injection rate, and other parameters, the nozzle geometry also controls the flow pattern created in the mold cavity. This flow pattern in turn controls the entrapment of inclusions and other defects which determine the steel quality.

3. THE PROBLEM

As shown in Fig. 1, the superheated jet of molten steel from the nozzle traverses across the mold cavity to impinge on the solidifying steel shell near the narrow faces. If the superheat is too large, the flow may break through the shell to create a costly breakout. The jets of molten steel exiting the nozzle also carry particles into the mold cavity in the form of oxide inclusions and argon bubbles, to which inclusions may attach. In addition, high speed flow across the top surface may shear droplets of liquid mold slag into the flow, where they may become entrained in the liquid steel.[31] If the flow pattern enables the particles to reach the top surface, they should be harmlessly removed into the liquid slag layer. However, when the flow pattern is detrimental, particles become entrapped in the solidifying steel shell, where they cause serious quality problems and costly rejects. Particles trapped near the meniscus generate surface delamination defects, and may initiate surface cracks. This occurs when the flow pattern generates excessive surface level fluctuations or insufficient liquid temperatures, so that particles are entrapped by the solidifying meniscus before they can enter the liquid slag. Particles which are entrained into the lower recirculation zones can gradually spiral and become trapped in the solidifying front deep inside the product,[15, 32] leading to internal cracks, slivers in the final rolled product, and blisters.[2] One of these

defects, known as "pencil pipes"[31] is caused when small argon gas bubbles surrounded by inclusions are caught in the solidifying shell. During rolling, the inclusion clusters elongate to create long slivers in the final product. During subsequent annealing processes, the trapped bubbles expand to create surface blisters.[31] These intermittent defects are particularly costly because they are often not detected until after many subsequent finishing steps. Thus, there is a great incentive to understand how to control the mold flow pattern in order to minimize particle entrapment and the associated quality problems.

4. PREVIOUS WORK

In previous work supported by this grant, and its industrial matching funds from the Continuous Casting Consortium at the University of Illinois, efforts have been made to develop and validate fluid flow modeling tools and to apply them to increase understanding and to improve the continuous casting process. Some of this recent work is summarized briefly below. More results and details are provided in the more than 30 publications resulting from this project to date [16-21, 24-30, 33-51] and in the website http://ccc.me.uiuc.edu. The flow modeling capability developed in this previous work is being extended to further fundamental and practical applications, which are briefly discussed in Section 5 of this paper.

A. Improved models of flow in continuous casting nozzles and mold

Several different computational models have been developed to simulate turbulent fluid flow and heat transfer in continuous casting nozzles and molds, including both large eddy simulations (LES) and conventional time-averaged models, (such as K-ε).[25-27] They have been applied to increase understanding, identify and quantify some of the transient features of the flow field in the continuous casting nozzle, mold, and slag layers, and how they interact. Modeling procedures for obtaining quantitative predictions have been identified. As an example, Fig. 2 compares the time-averaged flow pattern predicted from four different methods.[51] The transient simulation LES1 was computed with a refined Large Eddy Simulation model and the Smagorinsky subgrid scale model, while LES2 used a fine 1.5 million-node grid with no turbulence model (so is really DNS). The time-average results from a conventional K-ε model are similar, although it cannot predict the time-fluctuations properly. Figure 2 also compares this flow field with measurements obtained using Particle Image Velocimetry on a scale water model. [51] The importance of the transient nature of the flow on inclusion entrapment remains to be determined. The influence of inlet conditions into the mold on transient flow features has been studied. Specifically, accurate modeling of the nozzle flow to obtain better inlet conditions was found to change some flow features (such as increasing surface velocities) and better match with the PIV and plant measurements.

B. Benchmark experiments for continuous casting model validation

Experiments have been conducted to quantify fluid flow, superheat dissipation, solidifying steel shell growth, heat transfer and microstructure during the continuous casting of stainless-steel slabs at the AK Steel caster in Mansfield, OH.[52] These experimental measurements have further been applied to develop, calibrate, and validate mathematical models of both fluid flow and heat flow in continuous casting.[16]

Three-dimensional turbulent flow of molten steel in the nozzle and the mold cavity is modeled with the finite difference code CFX 4.2,[53] using the standard K-ε turbulence model and a fixed, structured grid. The results agree with flow measurements in a full-scale water model. The corresponding steady heat conduction equation is solved to predict the distribution of superheat in the molten pool. The predicted temperatures in the molten steel compare well with measurements conducted by inserting a thermocouple probe downward through the top surface at several locations in the operating thin slab caster. Next, solidification of the steel shell is simulated using a transient heat conduction model that features a detailed treatment of the flux layers in the interfacial gap and incorporates the superheat flux calculated from the fluid flow model. This model was calibrated with temperature measurements obtained from thermocouples in the copper mold during operation. It was run under the transient conditions present during a breakout. The predicted shell thickness profiles are compared with many shell thickness profiles measured around the perimeter of a breakout shell. Of greatest interest is the uneven thinning of the shell near the narrow face where the steel jet impinges, which is different between steady-state and the transient conditions of the breakout. This work provides a set of benchmark experiments for future continuous-casting model development. It further demonstrates the quantitative ability of this modeling approach to simulate coupled fluid flow and solidification heat conduction in a real steel continuous casting process.

C. Validation of flow using PIV and plant measurements

Measurements have been conducted to validate the ability of flow models to simulate turbulent, multiphase flow through the continuous casting nozzle.[18, 54] The experiments were conducted using particle image velocimetry on 0.4-scale physical water models of the process, using the PIV system at LTV Steel Technical Center. The measurements were also compared with both time-averaged (CFX) and transient (DNS / LES) models of flow in the mold.[24-29, 55] An example of the quantitative agreement is shown in Figure 2, as previously discussed. The computational results also compared favorably with velocity measurements in the operating steel caster, [51] using a pair of electromagnetic sensors embedded in the mold wall.[56] Calculations identified how the sensors are reliable only when placed near to the top surface, and when the flow direction is horizontal.[28] Flow fields in this molten metal process were compared using four different methodologies (steady K-ε and transient LES computations; PIV measurements in a water model; and electromagnetic sensor measurements in molten steel). More such studies are needed.

D. Nozzle model application: parametric studies

The validated nozzle model has been applied to perform a large, systematic study of the effect of important operating parameters on flow exiting the nozzle.[19, 54] Specifically, the jet characteristics (direction, speed, spread, etc.) exiting the nozzle ports are quantified for different operating parameters (nozzle bore diameter, slide gate orientation, slide gate opening fraction, injected fraction of argon gas, etc.). These results are a necessary first step in determining the important flow pattern in the mold.

E. Nozzle model application: argon gas flow optimization

The validated multiphase flow model of the nozzle was applied to perform over 150 simulations, in order to optimize argon gas injection levels in the nozzle for a range of practical conditions.[54] Specifically, the model results were processed (using simple inverse models) to quantify the minimum argon gas injection levels needed to avoid negative pressure in the nozzle, and thereby avoid air aspiration and the accompanying reoxidation, inclusion formation, and nozzle clogging. Increasing argon gas was found to generally increase nozzle pressure. Some conditions (low tundish level and low casting speed) required very little gas to avoid detrimental air aspiration, while other conditions (deep tundish) required more argon than is practical.[20] The model results can also be used as a clogging index to detect when nozzle clogging is present, before harmful flow defects occur. The implications of these results have been extended in a comprehensive review on how to avoid nozzle clogging.[21]

5. RESULTS

The present paper reports on some recent results from three different components of this multifaceted research project:

1) particle transport through a transient flow field

2) multiphase flow effects of argon gas bubble fraction and size distribution on flow in the mold

3) impinging jet transient flow and heat transfer

A. Particle Transport Study

Particles such as alumina inclusions, which are carried in with the jet entering the mold, may cause serious defects in the final steel product if they are not able to float harmlessly into the top-surface slag layer. The LES computations were extended to study both fluid flow and particle transport in the mold region of a full-scale water model[32] for conditions given in Table 1. Particle transport experiments[32] were performed in the water model by injecting 8000-30000 elliptical disk-shaped plastic beads with the water through the nozzle into the mold in each of at least five experiments. The density and size of the beads were chosen to match the vertical terminal velocity of 300mm alumina inclusions in molten steel. A screen was positioned near the top surface to trap the plastic beads and thereby simulate the removal of inclusion particles to the top surface. The average removal fraction was reported at different time intervals[32]. A hot-wire anemometer was used to measure the fluid velocity field.[11]

For inlet conditions, the LES flow model adopted velocity profiles from a prior simulation of fully-developed turbulent-flow in a pipe, rotated to the 25˚ downward inlet angle observed in the water model. After quasi-steady flow conditions were achieved in the strand water model, a large group of 15,000 particles was introduced at random locations on the inlet plane over a 1.6 s time interval. Six further groups of 500 particles each were then introduced every 2 seconds over 0.4s intervals. The particles were assumed to be spherical and were given initial velocities equal to the local instantaneous fluid velocity. Each particle trajectory was tracked during the transient flow simulation using a Lagrangian approach, by

integrating the particle transport equation with a fourth-order Runge-Kutta method at each time step, assuming a vertical buoyancy force according to the density difference and a drag force for particle Reynolds numbers up to 800.[57]

The computed fluid velocity field is very similar to the 0.4-scale water model results and agrees with flow observations of the full-scale water model.[11, 45] Figure 3 presents snapshots of the instantaneous distribution computed for the 15000 particles (group 0) at four different times after they were injected. The short line near the top surface represents the position of the screen. Neither the fluid flow nor the particle trajectory calculations are affected by the computational screen.

Figure 3 shows that the particles move with the jet after injection and start to impact the narrow face at about 1.6s. Next, they split into two groups and enter either the upper or lower recirculation rolls (Figure 3, 10s). Due in part to their buoyancy, many of the particles in the upper roll move to the top surface and are quickly and safely removed. Other particles circulate for a significant time (100s or more) before reaching the top surface to be removed. Finally, a few particles flow out of the mold bottom with the outflow and would be trapped at a deeper position, leading to defects in the real steel strand. Moreover, in a real steel caster, inclusion particles can also be entrapped by the solidifying shell (corresponding to the sidewalls of the water model). This was not modeled in either the water model or the computation.

Figure 4 shows the computed trajectories of four typical particles for 100 seconds, or until they contact the top surface (top left) or exit the domain (top right). The other two particles (lower frames) are still moving. These irregular trajectories show evidence of chaotic motion and illustrate the significant effect of the turbulent flow structures on particle transport, looking in both the wideface and narrow face directions.

The trajectory computations for the 15000-particles (group 0) were processed to compute the particle removal rate and removal fraction to the top surface (lines) in Figure 5 and to compare the computed and measured removal fractions by the screen (symbols). Removal is calculated by summing at each time step, the particles that touch either the top surface or the screen (from above). Considering the approximate nature of the experiments, and the uncertainties in the computations, the agreement between the computation and measurements appears to be quite good. Furthermore, the screen appears to simulate surface removal well at early times, but under-predicts it at later times (100s). The computation shows that the total removal rate appears to be very large (nearly 80%) when the walls do not trap particles. The initial positions of the particles in the nozzle port plane are found to be unrelated with their chance of removal to the top surface.

Finally, the computed particle removal fractions by the screen are compared in Table 2 with measurements. The removal rate of an individual group of 500 particles can be very different by a factor of over 1.5. This appears to be due to the sensitivity of the particle trajectories to transient variations in the flow field which persist over several seconds. However the average of 5 groups agrees with both the experiment and the 15000-particle group result. These results indicate that a large number of particles are required to study their transport (at least 2500 in this case), and that LES has the potential to accurately predict particle

trajectories and removal. Its main drawback is slow computational speed, as this single simulation of 140s required 39 days on a Pentium III 750 MHz PC for 175,000 time steps. Future work will investigate faster computational methods for parametric studies.

B. Multiphase Flow Study

Argon gas is often injected into the nozzle in order to prevent its clogging. This gas also has a great influence on flow in the strand. Increasing the amount of gas injection increases the buoyancy of the liquid jet, causing it to lift upward. Without gas, the classic "double roll" flow pattern is often produced, as studied in the previous section. Increasing the gas percentage above a critical level causes the flow pattern to change directions, forming a "single-roll" flow pattern, where the flow across the top surface is directed away from the SEN. This transition in flow patterns was studied using both water models and steady K-ε computations. In this work, a single set of conditions was studied, given in Table 3. This case was chosen because previous work had discovered discrepancies for these particular conditions between the flow patterns found in a 0.4-scale water model and in the actual caster, as measured both by electromagnetic sensors in the mold wall and as inferred by the shape of the slag layer.[58]

To model two-phase flow, an additional set of momentum conservation equations was solved for the argon gas phase. Interphase coupling terms were added to the liquid momentum equations to account for the drag in proportion to the relative velocities of the liquid and bubble phases, which were generally in the Stokes or Allen regimes. The results depend greatly on the bubble size,[11] which in reality has a distribution that can evolve with the flow. In this work, these complex phenomena were treated by first characterizing the bubble size distribution as having eleven different discrete sizes, (0.5mm, 1.5mm, …, 10.5 mm) each with its own volume fraction, according to the Multiple Size Group model in CFX [53]. In this model, the average bubble velocity is related to the “Sauter” mean diameter of the distribution, in order to solve only a single additional set of gas momentum equations. Additional continuity equations are solved for each size group, to represent the size distribution. Furthermore, the initial bubble volume fractions, imposed at the nozzle port, were subjected to evolution, according to the binary breakup model of Luo and Svendsen [59], assuming a breakup coefficient of 0.1. Coalescence was assumed to be small (due to surface tension repulsion), by setting the coalescence coefficient [53] to 0.

The most difficult aspect of setting up the computational modeling was determination of the bubble size distribution. (Large numbers of small bubbles provide more drag than small numbers of large bubbles, so their buoyancy is able to exert more lift onto the flow pattern). The diameters of individual bubbles were measured from still photographs of the operating water model and compiled into a volume fraction distribution. Bubble sizes in the caster were estimated by extrapolating size distributions measured in a water model of a nozzle where vertical flow generated bubbles via shear. The results were adjusted for steel / argon properties by applying the mathematical model of Bai,[54] assuming about 200 active sites for gas emission from the 78 mm bore x 50 mm high cylindrical surface area of the porous ceramic wall. The resulting size distributions for the water model and steel caster are compared in Figure 6. Bubbles in the

water model are seen to have wide size variations, owing to the single, annular-shaped inlet area, which generates relatively large, elongated bubbles. The steel caster is expected to have more uniformly-sized bubbles, owing to the stable shear-driven formation mechanism expected for this low gas flow rate per pore.

The computation begins by first solving for flow in the nozzle, as shown in Figure 7. This figure illustrates how gas concentrates in the upper portion of the exit plane of the nozzle port, where the velocity, K, and ε distributions are used to define the inlet conditions for the strand simulation. The calculated flow pattern in the strand water model is compared with the velocity distribution measured using Particle Image Velocimetry in Figure 8. Both results agree that a consistent "single-roll" flow pattern is produced for these conditions, despite a few minor discrepancies with the inlet conditions. The jet is quickly buoyed up to the top surface owing to its argon gas content, and it flows along the top surface away from the SEN.

The computational model was next applied to simulate the flow pattern measured in the steel caster for approximately the same conditions. The steel caster is different from the water model in several important ways. Changes to this simulation, given in Table 3 include:

-increasing the dimensions by a factor of 2.5 to simulate the full-scale geometry;

-increasing the inlet velocities by a factor of 1.581 (to simulate the actual casting speed rather than the velocities in the water model, which were scaled down according to the standard modified Froude criterion);

-replacing the domain bottom with a pressure boundary condition;

-changing the bubble distribution (Figure 6); and

-changing the liquid properties.

Figure 9 shows results for both velocity vectors and gas distribution in top view and side view slices through both the centerline and near to the wide face. The flow pattern is not symmetrical, owing to the swirling flow exiting the nozzle port that was imparted by the slide gate. The results generally exhibit classic double-roll flow behavior. The jet is quite shallow, but the flow pattern is consistently towards the SEN along the top surface. The jet first impinges on the narrow face. The bubble contours all stay within the upper recirculation zone, indicating that bubble entrapment into the lower roll should be rare. The flow pattern measured in the plant is also a double-roll flow pattern for this case,[58] which is consistent with these predictions. However, the plant measurements also show that the flow pattern sometimes experiences transition flow states, where the flow direction reverses inconsistently, and correlates with casting defects.[58] This might be caused by transient structures breaking off from the jet, which is predicted to be quite shallow and near to the surface. Especially if the nozzle submergence becomes shallower, or if the bubble size decreased or gas fraction increased, it is not surprising from the simulation that this flow pattern might exhibit detrimental transition behavior.

The most significant finding of this study is that the flow pattern in the steel caster is sometimes very different from that in a scale water model and that the steady, multiphase K-ε computation can match both. Specifically, the flow pattern reverses from a stable single-roll flow pattern in the 0.4-scale water model to an unstable double-roll flow pattern in the full-size caster. Of the many causes for this difference, the most important is likely the reduced-scale of the water model combined with the Froude-based velocity scaling criterion. Further parametric studies with the computational model are planned to determine the upper limit for argon injection that still produces a stable double-roll flow pattern and avoids the detrimental transition flow pattern.

C. Impinging Jet Study

A separate set of computations is being carried out to study the transient flow fields and rates of heat transfer under jets impinging on a solid surface. The objective of these studies is to evaluate the ability of LES to predict heat transfer rates for impinging jets. This is important for the prediction of shell thinning and breakouts. The calculations are initially being conducted for air as the fluid in order to compare the results with other experimental data. Calculations have been made of a circular jet impinging on a flat surafce. The jet Reynolds number is varied from 5000 to 60,000. A turbulent flow field in a pipe is first computed. This is then prescribed as an inlet condition to the impinging jet computation. The radius of the domain is taken to be 16 times the radius of the jet. At the outlet to the domain, the velocities are prescribed. A grid consisting of 128 x 64 x 128 cells was used for these computations.

Results from calculations at Reynolds number of 5000 are shown in Figs. 10 and 11. The time averaged Nusselt number is shown as a function of the radius. The agreement with heat transfer measurements is very good, indicating the benefits a well-resolved LES calculation. An instantaneous flow field, shown in Fig. 10, illustrates the large-scale turbulence structures in the impinging jet. The angle of jet impingement against the narrow face also appears to have an important influence on the fraction of inclusion particles transported down deep into the caster, where they may become entrapped to form defects.

We now have developed a new algorithm and LES code that can compute more general flows. This code is being applied to compute planar impinging jets, as more relevant to the continuous casting situation. These calculations are underway, but have not been completed. The future plan is to study the effect of the jet angle on the heat transfer rates, by conducting LES of obliquely impinging jets. Special wall functions that may be important to accurately obtaining heat transfer rates for high Reynolds numbers will be developed.

6. SIGNIFICANT FINDINGS

Several different computational models of turbulent fluid flow and heat transfer have been developed to simulate flow phenomena in the nozzle and mold regions of the continuous casting of steel slabs. The models are being calibrated, validated, and tested through water model experiments, steel plant trials, and metallographic measurements at LTV Steel and several other steel companies who are cosponsoring this research. LES model predictions have identified important time-dependent flow features, which match

water model measurements. Time-average flow fields with both LES and k-ε models roughly agree with both water model and steel caster measurements for single-phase flow. Recent k-ε model simulations with multiple bubble size distributions have shown differences between multiphase flow in a 0.4-scale water model and flow in the steel caster. Separate predictions have matched measurements in both systems. In addition to the inlet velocity and direction, the turbulence and swirl at the inlet ports has been shown to be very important to both the fluid flow and inclusion motion.

7. IMPACT

This work aims to improve understanding of transient flow, inclusion transport and defect formation in the mold region during the continuous casting of steel slabs, through the development, validation, and application of fundamental computational models of transient fluid flow. Plant observations have found that many serious quality problems, including inclusion entrapment, are directly associated with the flow pattern in the mold. The results from the computational simulations of this work are increasing fundamental understanding of transient fluid flow, gas, and inclusion particle transport in the mold region. This will lead to optimized nozzle geometry and gas flow rates to improve mold flow patterns and minimize inclusion defects. Lowering defects from internal inclusions can improve steel minimum strength, fatigue life, surface appearance, yield and energy efficiency (from reduced rejects) and lower production cost. Furthermore, the computational tools developed and validated in this work can be applied to study and optimize flow in other processes.

8. ACKNOWLEDGEMENTS

The authors wish to thank students Quan Yuan, Tiebiao Shi, and Bin Zhao for results referred to in this paper and for help with preparation of figures. Funding from the National Science Foundation (Grants # DMI-98-00274 and DMI-01-15486) and the Continuous Casting Consortium (Accumold, Huron Park, Ontario; Allegheny Ludlum Steel, Brackenridge, PA; AK Steel, Middletown, OH; Columbus Stainless Steel, Middelburg, South Africa; LTV Steel Co., Cleveland, OH; Hatch Associates, Buffalo, New York; and Stollberg, Niagara Falls, NY) is gratefully acknowledged. Finally, thanks are due to the National Center for Supercomputing Applications at the University of Illinois for computing time and use of the CFX and FLUENT codes.

9. REFERENCES

1. "Continuously Cast Steel Output, 1999," Report, International Iron Steel Institute, Brussels, Belgium, 2000, www.worldsteel.org.

2. J. Herbertson, Q.L. He, P.J. Flint, R.B. Mahapatra, "Modelling of Metal Delivery to Continuous Casting Moulds," in Steelmaking Conf. Proc., Vol. 74, ISS, Warrendale, PA, (Washington, D.C.), 1991, 171-185.

3. T. Honeyands and J. Herbertson, "Oscillations in Thin Slab Caster Mold Flows," 127th ISIJ Meeting, ISIJ, Tokyo, Japan, 1994.

4. B.G. Thomas, "Application of Mathematical Models to the Contious Slab Casting Mold.," Iron & Steelmaker (ISS Trans.), Vol. 16 (12), 1989, 53-66.

5. B.G. Thomas, "Mathematical Modeling of the Continuous Slab Casting Mold, a State of the Art Review," in Mold Operation for Quality and Productivity, A. Cramb, ed. Iron and Steel Society, Warrendale, PA, 1991, 69-82.

6. B.G. Thomas and F.M. Najjar, "Finite-Element Modeling of Turbulent Fluid Flow and Heat Transfer in Continuous Casting," Applied Mathematical Modeling, Vol. 15 (5), 1991, 226-243.

7. X. Huang, B.G. Thomas and F.M. Najjar, "Modeling Superheat Removal during Continuous Casting of Steel Slabs," Metall. Trans. B, Vol. 23B (6), 1992, 339-356.

8. X. Huang and B.G. Thomas, "Modeling of Steel Grade Transition in Continuous Slab Casting Processes," Metall. Trans., Vol. 24B (2), 1993, 379-393.

9. D.E. Hershey, B.G. Thomas and F.M. Najjar, "Turbulent Flow through Bifurcated Nozzles," Int. J. Num. Meth. in Fluids, Vol. 17 (1), 1993, 23-47.

10. B.G. Thomas and X. Huang, "Effect of Argon Gas on Fluid Flow in a Continuous Slab Casting Mold," in 76th Steelmaking Conf. Proc., Vol. 76, Iron and Steel Society, Warrendale, PA, (Dallas, TX), 1993, 273-289.

11. B.G. Thomas, X. Huang and R.C. Sussman, "Simulation of Argon Gas Flow Effects in a Continuous Slab Caster," Metall. Trans. B, Vol. 25B (4), 1994, 527-547.

12. G.D. Lawson, S.C. Sander, W.H. Emling, A. Moitra, B.G. Thomas, "Prevention of Shell Thinning Breakouts Associated with Widening Width Changes," in Steelmaking Conf. Proc., Vol. 77, ISS, Warrendale, PA, (Chicago, IL), 1994, 329-336.

13. F.M. Najjar, B.G. Thomas and D.E. Hershey, "Turbulent Flow Simulations in Bifurcated Nozzles: Effects of Design and Casting Operation," Metall. Trans. B, Vol. 26B (4), 1995, 749-765.

14. R. McDavid and B.G. Thomas, "Flow and Thermal Behavior of the Top-Surface Flux/ Powder Layers in Continuous Casting Molds," Metall. Trans. B, Vol. 27B (4), 1996, 672-685.

15. B.G. Thomas, A. Denissov and H. Bai, "Behavior of Argon Bubbles during Continuous Casting of Steel," in Steelmaking Conf. Proc., Vol. 80, ISS, Warrendale, PA., (Chicago, IL), 1997, 375-384.

16. B.G. Thomas, R. O'Malley, T. Shi, Y. Meng, D. Creech, D. Stone, "Validation of Fluid Flow and Solidification Simulation of a Continuous Thin Slab Caster," in Modeling of Casting, Welding, and Advanced Solidification Processes, Vol. IX, Shaker Verlag GmbH, Aachen, Germany, (Aachen, Germany, August 20-25, 2000), 2000, 769-776.

17. H. Bai and B.G. Thomas, "Bubble Formation during Horizontal Gas Injection into Downward Flowing Liquid," Metall. Mater. Trans. B, 2001, in press.

18. H. Bai and B.G. Thomas, "Turbulent Flow of Liquid Steel and Argon Bubbles in Slide-Gate Tundish Nozzles, Part I, Model Development and Validation," Metall. Mater. Trans. B, Vol. 32B (2), 2001, 253-267.

19. H. Bai and B.G. Thomas, "Turbulent Flow of Liquid Steel and Argon Bubbles in Slide-Gate Tundish Nozzles, Part II, Effect of Operation Conditions and Nozzle Design," Metall. Mater. Trans. B, Vol. 32B (2), 2001, 269-284.

20. H. Bai and B.G. Thomas, "Effects of Clogging, Argon Injection and Continuous Casting Conditions on Flow and Air Aspiration in Submerged Entry Nozzles," Metall. Mater. Trans. B, Vol. 32B (4), 2001, 707-722.

21. B.G. Thomas and H. Bai, "Tundish Nozzle Clogging – Application of Computational Models," in Steelmaking Conf. Proc., Vol. 18, Iron and Steel Society, Warrendale, PA, (Baltimore, MD), 2001, 895-912.

22. B.G. Thomas, "Modeling Study of Intermixing in Tundish and Strand during a Continuous-Casting Grade Transition," Iron and Steelmaker, Vol. 24 (12), 1997, 83-96.

23. X. Huang and B.G. Thomas, "Modeling of Transient Flow Phenomena in Continuous Casting of Steel," Canadian Metall. Quart., Vol. 37 (304), 1998, 197-212.

24. B.G. Thomas, H. Bai, S. Sivaramakrishnan, S.P. Vanka, "Detailed Simulation of Flow in Continuous Casting of Steel Using K-ε, LES, and PIV," International Symposium on Cutting Edge of Computer Simulation of Solidification and Processes, (Osaka, Japan, Nov. 14-16, 1999), ISIJ, 1999, 113-128.

25. B.G. Thomas and S.P. Vanka, "Study of Transient Flow Structures in the Continuous Casting of Steel," NSF Design & Manufacturing Grantees Conference, (Long Beach, CA), NSF, Washington, D.C., 1999.

26. B.G. Thomas and S.P. Vanka, "Study of Transient Flow Structures in the Continuous Casting of Steel," NSF Design & Manufacturing Grantees Conference, (Vancouver, Canada), NSF, Washington, D.C., 2000, 14p.

27. S.P. Vanka and B.G. Thomas, "Study of Transient Flow Structures in the Continuous Casting of Steel," NSF Design & Manufacturing Grantees Conference, (Jan. 7-10, Tampa, FL), NSF, Washington, D.C., 2001, 14p.

28. S. Sivaramakrishnan, H. Bai, B.G. Thomas, P. Vanka, P. Dauby, M. Assar, "Transient Flow Structures in Continuous Cast Steel," in Ironmaking Conference Proceedings, Vol. 59, ISS, Warrendale, PA, (Pittsburgh, PA), 2000, 541-557.

29. S. Sivaramakrishnan, B.G. Thomas and S.P. Vanka, "Large Eddy Simulation of Turbulent Flow in Continuous Casting of Steel," in Materials Processing in the Computer Age, Vol. 3, V. Voller and H. Henein, eds., TMS, Warrendale, PA, 2000, 189-198.

30. B.G. Thomas, "Modeling of the Continuous Casting of Steel: Past, Present, and Future," in Electric Furnace Conf. Proc., Vol. 59, ISS, Warrendale, PA, (Phoenix, AZ), 2001.

31. W.H. Emling, T.A. Waugaman, S.L. Feldbauer, A.W. Cramb, "Subsurface Mold Slag Entrainment in Ultra-Low Carbon Steels," in Steelmaking Conf. Proc., Vol. 77, ISS, Warrendale, PA, (Chicago, IL), 1994, 371-379.

32. R.C. Sussman, M. Burns, X. Huang, B.G. Thomas, "Inclusion Particle Behavior in a Continuous Slab Casting Mold," in 10th Process Technology Conference Proc., Vol. 10, Iron and Steel Society, Warrendale, PA, (Toronto, Canada, April 5-8, 1992), 1992, 291-304.

33. B.G. Thomas, "Mathematical Models of Continuous Casting of Steel Slabs," Report, Continuous Casting Consortium, University of Illinois at Urbana-Champaign, 1999.

34. B.G. Thomas, "University - Steel Industry Interaction, R&D in the Steel Industry," 40th Congreso Latinoamericano de Siderurgia, ILAFA 40 Congress Proceedings, (Buenos Aires, Argentina), Inst. Argentino de Siderurgia, 1999, 65-67.

35. Y. Miki and B.G. Thomas, "Modeling of Inclusion Removal in a Tundish," Metall. Mater. Trans. B, Vol. 30B (4), 1999, 639-654.

36. B.G. Thomas, "Mathematical Models of Continuous Casting of Steel Slabs," Report, Continuous Casting Consortium, University of Illinois at Urbana-Champaign, 2000.

37. B.G. Thomas, "The Importance of Numercial Simulations for Further Improvements of the Continuous casting Process," 8th International Continuous Casting Conference, (Linz, Austria, August 20-25, 2000), Voest Alpine, Linz, Austria, 2000, 7.1-7.11.

38. H. Bai and B.G. Thomas, "Effect of Clogging, Argon Injection, and Casting Conditions on Flow Rate and Air Aspiration in Submerged Entry Nozzles Steel," in 83rd Steelmaking Conf. Proc., Vol. 83, ISS, Warrendale, PA, (Pittsburgh, PA, March 2-29, 2000), 2000, 183-197.

39. H. Bai and B.G. Thomas, "Two-Phase Flow in Tundish Nozzles During Continuous Casting of Steel," in Materials Processing in the Computer Age, Vol. 3, V. Voller and H. Henein, eds., TMS, Warrendale, PA, 2000, 85-99.

40. B.G. Thomas, "Continuous Casting," in The Encyclopedia of Materials: Science and Technology, Vol. 2, D. Apelian, ed. Elsevier Science Ltd., Oxford, UK., 2001, 6p.

41. B.G. Thomas, "Fundamentals of Continuous Casting: Modeling," in Making, Shaping and Treating of Steel: Continuous Casting, Vol. 5, A. Cramb, ed. AISE Steel Foundation, Pittsburgh, PA, 2001, Chapter 3.9, submitted Oct., 2000.

42. B.G. Thomas, "Continuous Casting Operation: Fluid Flow," in Making, Shaping and Treating of Steel: Continuous Casting, Vol. 5, A. Cramb, ed. AISE Steel Foundation, Pittsburgh, PA, 2001, Chapter 4.3, submitted Oct., 2000.

43. B.G. Thomas, "Continuous Casting of Steel, Chap. 15," in Modeling and Simulation for Casting and Solidification: Theory and Applications, O. Yu, ed. Marcel Dekker, New York, 2001, 499-539.

44. T. Shi and B.G. Thomas, "Effect of Gas Bubble Size on Fluid Flow in Continuous Casting Mold," Report, Continuous Casting Consortium, 2001.

45. Q. Yuan, S.P. Vanka and B.G. Thomas, "Large Eddy Simulations of Turbulent Flow and Inclusion Transport in Continuous Casting of Steel," 2nd International Symposium on Turbulent and Shear Flow Phenomena, June 27 - 29, 2001, Royal Institute of Technology (KTH), Stockholm, Sweden, 2001, 6.

46. C. Bernhard, B.G. Thomas, G. Xia, C. Chimani, "Simulation of Solidification and Microstructure in Continuous Casting," Berg- und Huettenmaennische Monatshefte, 2001, submitted, June, 2001.

47. Q. Yuan, T. Shi, B.G. Thomas, S.P. Vanka, "Simulation of Fluid Flow in the Continuous Casting of Steel," Computational Modeling of Materials, Minerals and Metals Processing, (San Diego, CA), TMS, Warrendale, PA, 2001, 10p.

48. Q. Yuan, S. Sivaramakrishnan, S.P. Vanka, B.G. Thomas, "Large Eddy Simulations of Turbulent Flow Structures in Continuous Casting of Steel," Metall. Mater. Trans., 2001, submitted July 8, 2001.

49. B.G. Thomas, "Continuous Casting: Modeling," in The Encyclopedia of Advanced Materials, Vol. 2, A.G. J. Dantzig, J. Michalczyk, ed. Pergamon Elsevier Science Ltd., Oxford, UK, 2001, 8p, in press.

50. B.G. Thomas and L. Zhang, "Mathematical Modeling of Fluid Flow in Continuous Casting: a Review," ISIJ Internat., Vol. 41 (10), 2001, 1185-1197.

51. B.G. Thomas, Q. Yuan, S. Sivaramakrishnan, T. Shi, S.P. Vanka, M.B. Assar, "Comparison of Four Methods to Evaluate Fluid Velocities in a Continuous Casting Mold," ISIJ Internat., Vol. 41 (10), 2001, 1266-1276.

52. B.G. Thomas, R.J. O'Malley and D.T. Stone, "Measurement of temperature, solidification, and microstructure in a continuous cast thin slab," Modeling of Casting, Welding, and Advanced Solidification Processes, (San Diego, CA), TMS, Warrendale, PA, Vol. VIII, 1998, 1185-1199.

53. CFX 4.2, Report, AEA Technology, 1700 N. Highland Rd., Suite 400, Pittsburgh, PA 15241, 1998.

54. H. Bai, "Argon Bubble Behavior in Slide-Gate Tundish Nozzles During Continuous Casting of Steel Slabs," PhD Thesis, University of Illinois, 2000.

55. S. Sivaramakrishnan, "Transient Fluid Flow in the Mold and Heat Transfer Through the Molten Slag Layer in Continuous Casting of Steel," M.S. Thesis, University of Illinois, 2000.

56. P. Andrzejewski, D. Gotthelf, E. Julius, H. Haubrich, "Mould Flow Monitoring at No. 3 Slab Caster, Krupp Hoesch Stahl AG," in Steelmaking Conf. Proc., Vol. 80, ISS, Warrendale, PA, 1997, (Chicago, IL), 1997, 153-157.

57. L. Shiller and A. Naumann, "Uber die grundlegenden Berechungen bei der Schwerkraftaufbereitung," Ver. Deut. Ing., Vol. 77, 1933, 318.

58. M.B. Assar, P.H. Dauby and G.D. Lawson, "Opening the Black Box: PIV and MFC Measurements in a Continuous Caster Mold," in Steelmaking Conf. Proc., Vol. 83, ISS, Warrendale, PA, (Pittsburgh, PA), 2000, 397-411.

59. H. Luo and H.F. Svendsen, "Theoretical model for drop and bubble breakup in turbulent dispersions," AICHE J., Vol. 42 (5), 1996, 1225-1233.

Table 1. Conditions for the full-scale water model measurements and simulation.

	Experiment	LES simulation
Nozzle port size /Inlet port size (x × y) (m)	0.051 × 0.056	0.051 × 0.056
Submergence depth (m)	0.150	0.150
Nozzle angle	25^o	25^o
Inlet jet angle	25^o	25^o
Mold /Domain height (m)	2.152	2.152
Mold /Domain width (m)	1.83	0.965
Mold /Domain thickness (m)	0.238	0.238
Average inlet flow rate (m^3/s)	0.00344	0.00344
Average inlet speed (m/s)	1.69	1.69
Fluid density (kg/m^3)	1000	1000
Casting speed (m/s)	0.0152	0.0152
Fluid kinematic viscosity (m^2/s)	1.0×10^{-6}	1.0×10^{-6}
Particle inclusion size (mm)	2 – 3	3.8 (diameter)
Particle inclusion density (kg/m^3)	988	988
Corresponding alumina inclusion diameter in steel caster (μm)	300	300

Table 2: Comparison of particle removal by screen.

		0-10 seconds	10-100 seconds
LES	500 particle groups		
	1	27.2%	23.4%
	2	17.8%	27.2%
	3	26.2%	23.0%
	4	23.8%	23.2%
	5	33.0%	18.2%
	Average	25.56%	23.0%
	15000 particles (group 0)	26.96%	26.03%
Experiment		22.3%	27.6%

Table 3. Multiphase Flow Model Conditions

	0.4-scale Water Model	Steel Caster
Mold Width x Thickness	730 x 80 mm	1854 x 228 mm
Mold / Strand Height	950 mm	open bottom
Nozzle Submergence Depth (top surface to top of port)	80 mm	165 mm (6.5 inch)
Nozzle Bore Inner Diameter	31 mm	80 mm
Port Wall Thickness	11mm	27.5 mm
Nozzle Port Height x Width	31 x 31 mm	78 x 78 mm
Nominal Vertical Angle of Port Edges	15° down	15° down
Jet Angle: vertical, horizontal	30˚ down 0˚	10.1˚ down 12.1˚
Average Inlet Velocities, V_x, V_z	0.358 m/s, 0.207 m/s	0.562 m/s, 0.324 m/s
Inlet Turbulent Kinetic Energy, K_o	0.044 m^2/s^2	0.193 m^2/s^2 avg.
Inlet Turbulence Dissipation Rate, ε_o	0.999 m^2/s^3	3.037 m^2/s^3 avg.
Liquid Density, ρ	1000 kg/m^3	7020 kg/m^3
Liquid Laminar Viscosity, μ_o	0.001 kg/m-s	0.0056 kg/m-s
Casting Speed, V_c	Froude similarity	14.8 mm/s (35’’/min)
Liquid Flow Rate (whole slab)	0.0378 m^3/min	0.376 m^3/min
Gas Flow Rate (cold) (hot)	 3.71 SLPM	6.3 SLPM 34.9 SLPM
Gas Volume Fraction, f_{gas}	8.9 %	8.5%
Bubble diameter (avg)	2.43 mm	2.59 mm

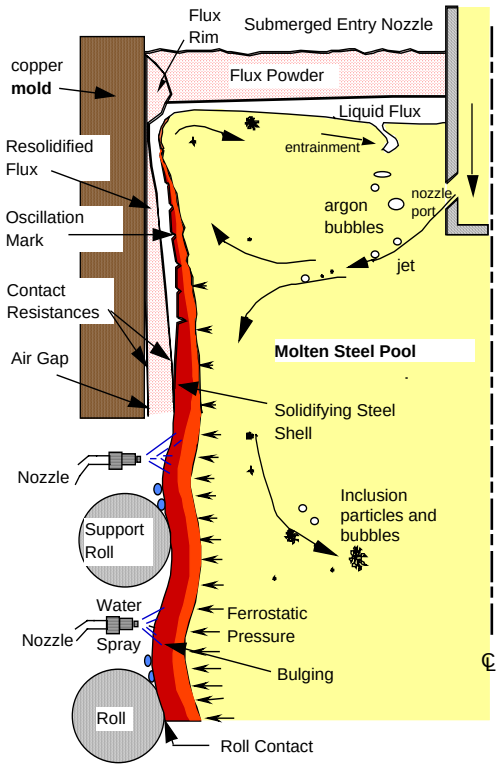

Figure 1: Schematic of flow phenomena in mold region of continuous casting process.

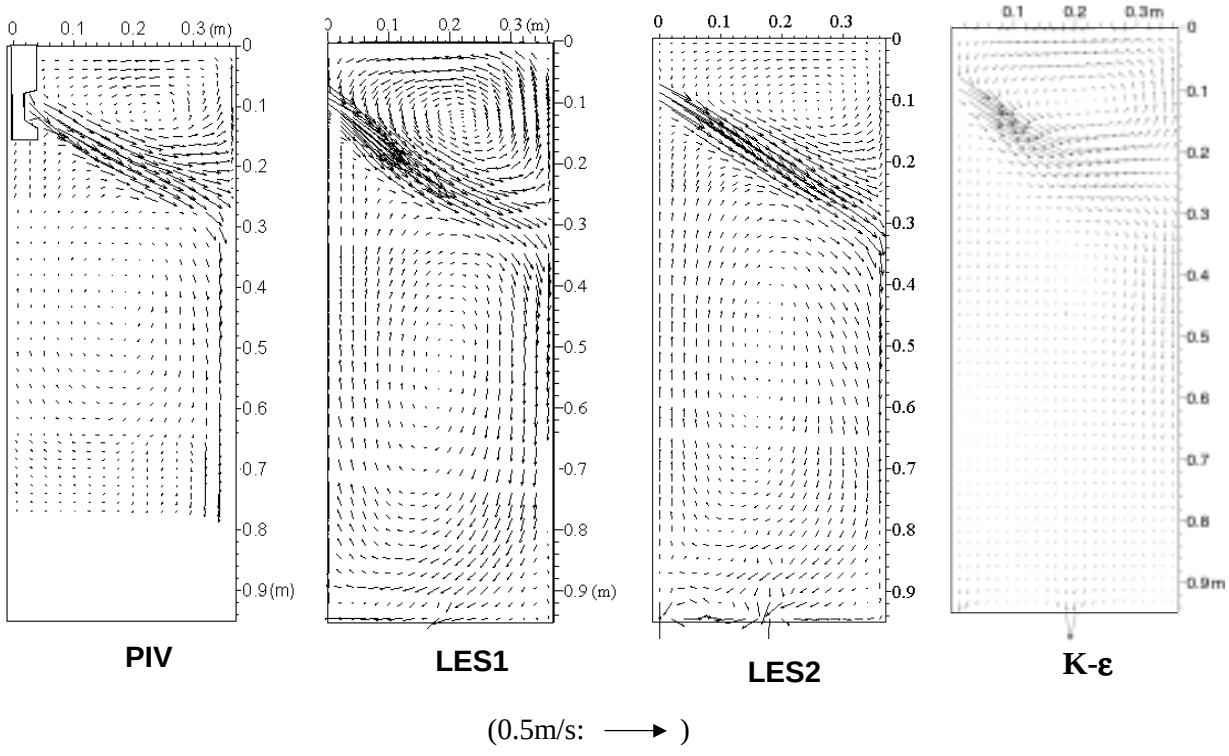

Figure 2: Comparison of time-average flow pattern in mold centerplane from 4 methods.

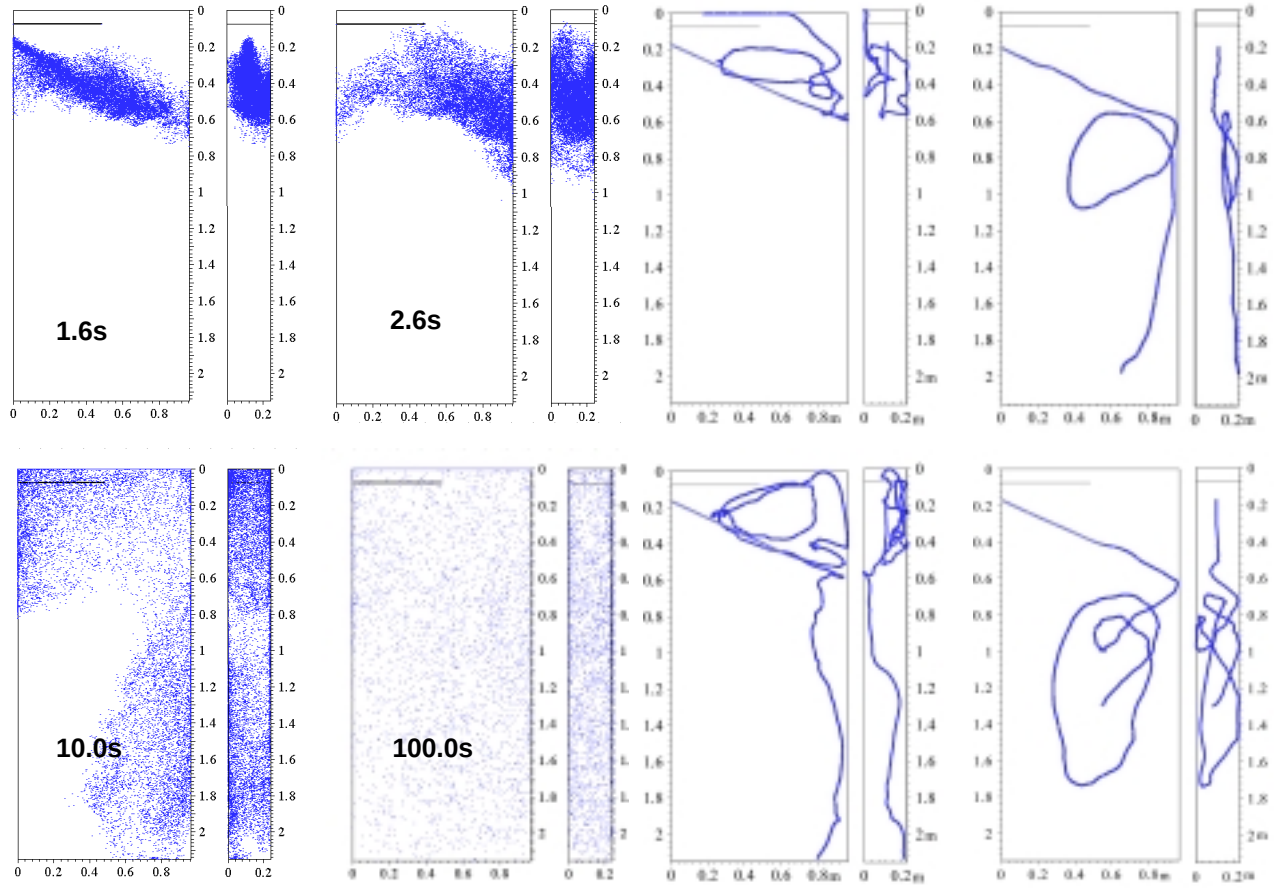

Figure 3: Distribution of the 15000 particles at four instants after their injection.

Figure 4: Four typical particle trajectories found in the computation.

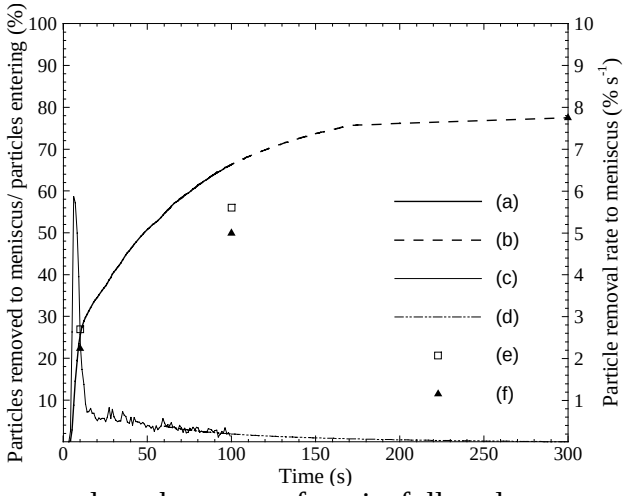

Figure 5: Particle removal to the top surface in full-scale water model: (a) particles removed to top surface (simulated); (b) particles removed to top surface; (c) particle removal rate to top surface; (d) particle removal rate to top surface; (e) particles removed by screen (LES); (f) particles removed by screen (experiment).

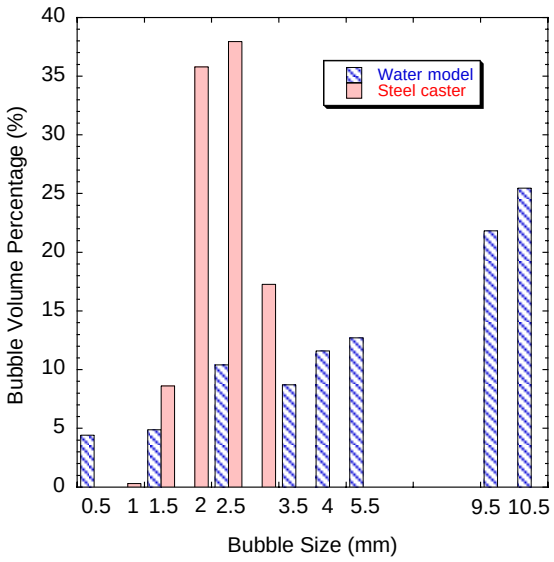

Figure 6: Bubble distributions entering water model and steel caster.

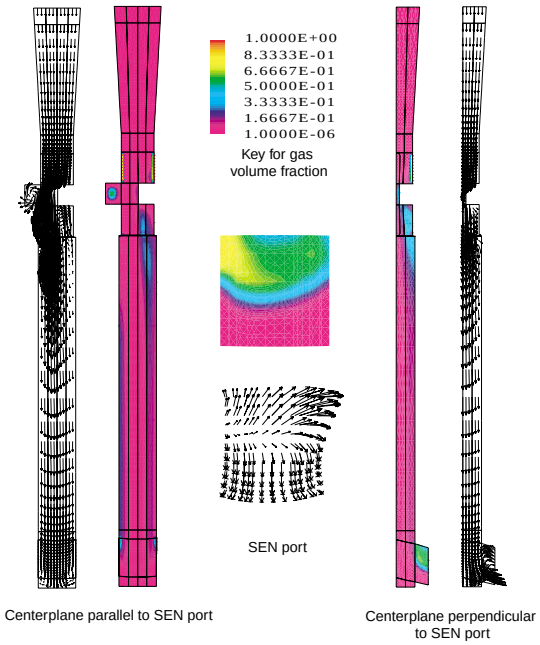

Figure 7: Computed steel velocity and gas volume fraction in nozzle.

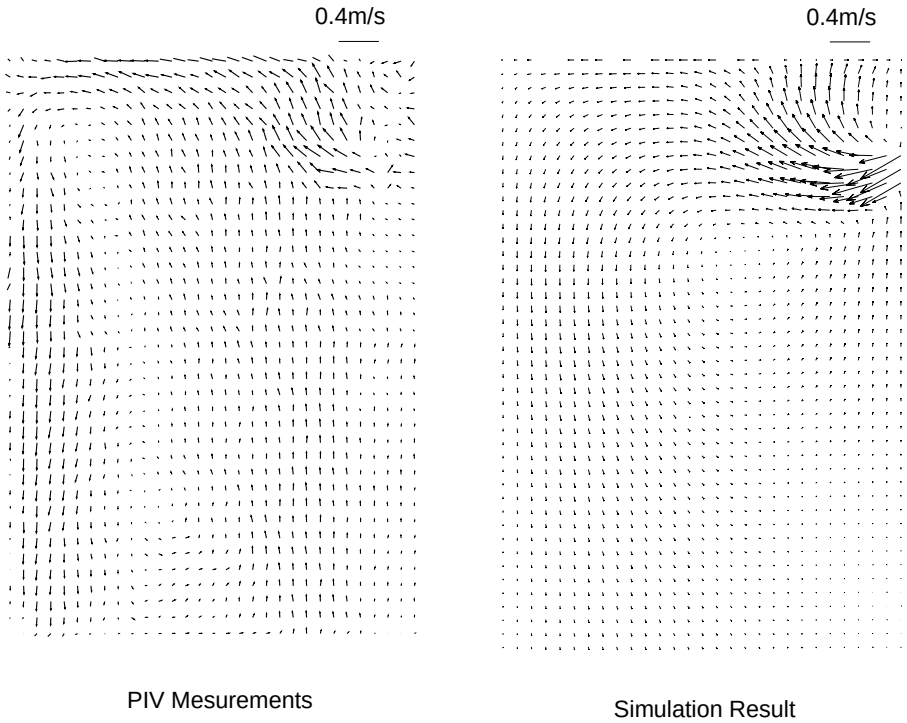

Figure 8: PIV measurements and computed velocity vectors of multiphase flow in 0.4-scale water model centerplane (Table 3 conditions).

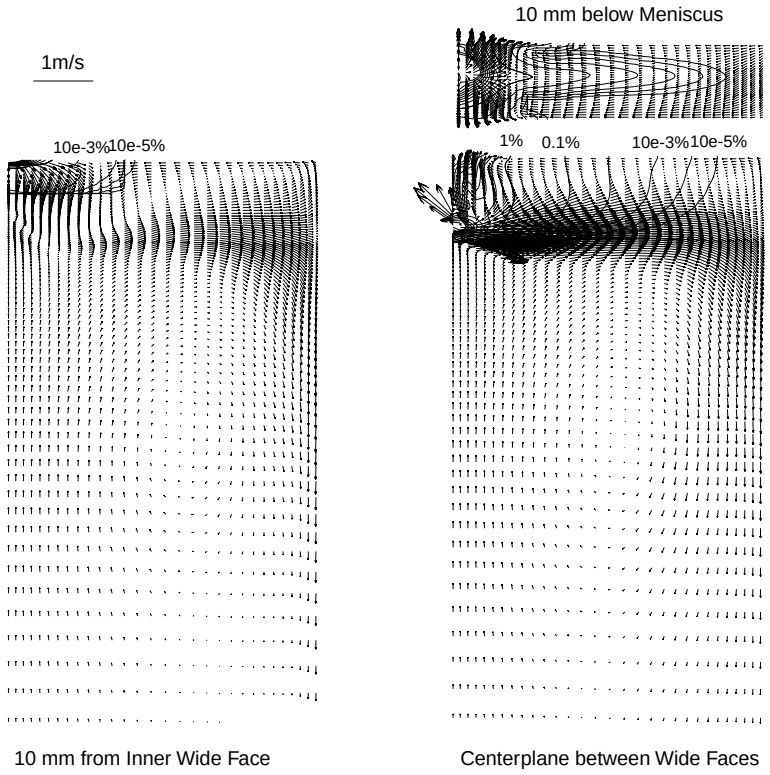

Figure 9: Computed velocities in steel caster.

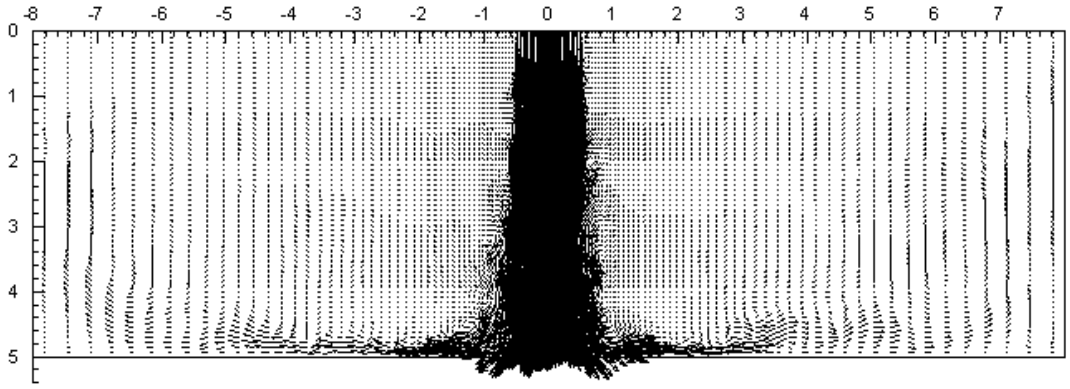

Figure 10: Instantaneous velocity field.

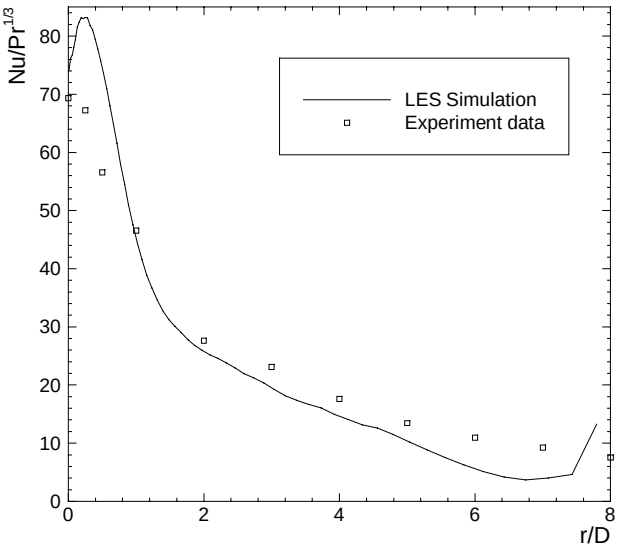

Figure 11: Mean Nusselt number.